NATURAL SCIENCE REVIEW 2 100401 (2025)
nsr.jinr.int

Comparative analysis of enriched mesenchymal stem cells conditioned medium fractions obtained by ultrafiltration

E. Andreev[1], E. Kravchenko*[1], E. Zavyalova[1,2], P. Eremin[3], A. Rzyanina[1], P. Markov[3], and A. Nechaev[1]

[1] *Joint Institute for Nuclear Research, Dubna, Russia*
[2] *Chemistry Department, Lomonosov Moscow State University, Moscow, Russia*
[3] *National Medical Research Center for Rehabilitation and Balneology of the Ministry of Health of the Russian Federation, Moscow, Russia*

Abstract

This study provides a comparative analysis of various components of mesenchymal stem cells (MSC) conditioned media (CM) obtained using serum-containing and serum-free culture methods, revealing significant differences in their composition and potential clinical applicability. Serum-containing CM exhibits significantly higher levels of total protein, non-vesicular RNA, exosomes, and nanoparticles compared to serum-free CM, reflecting the contribution of both the MSC secretome and residual fetal bovine serum components. Ultrafiltration-based fractionation (0.2 μm–50 kDa) allows the isolation of fraction enriched in exosomes and proteins, preserving the functionally significant components of the MSC secretome. This strategy effectively captures small vesicles and mid-sized proteins while excluding larger or smaller biomolecules, enhancing utility for targeted analyses. The presented data underscore the need for context-driven CM selection and provide information for choosing the optimal strategy for obtaining the MSC secretome balancing yield, purity, and regulatory demands in MSC research and therapy.

Keywords: MSC, secretome, conditioned media, serum-free culture, exosome isolation, ultrafiltration

DOI: 10.54546/NaturalSciRev.100401

1. Introduction

Mesenchymal stem cells have attracted considerable attention in regenerative medicine and biotechnology due to their ability to undergo multipotent differentiation and paracrine effects. One of the key mechanisms through which MSC exert their influence is the external secretion of bioactive molecules and extracellular vesicles (EVs), and the secretome profile released into conditioned media varies with the MSC source (bone marrow, adipose tissue), culture conditions, and stimulation (inflammatory priming), influencing downstream effects [1].

*Corresponding author e-mail address: elenakravchenko@jinr.ru

Received: 22 April 2025; Revised: 13 June 2025; Accepted: 18 June 2025; Published: 2 July 2025
Copyright: © by the author(s), 2025, under license to Joint Institute for Nuclear Research. This article is an open access article distributed under the terms and conditions of the Creative Commons Attribution-NonCommercial 4.0 International license (CC BY-NC License 4.0).

MSC-produced conditioned media is a complex cocktail of paracrine factors, including growth factors (e.g., VEGF, HGF), cytokines (e.g., IL-6, IL-10), and EVs, particularly exosomes [2]. Exosomes, 30–150 nm vesicles carrying proteins, lipids, and nucleic acids (miRNAs, mRNAs), play a key role in intercellular communication by transferring molecules into recipient cells. These vesicles are involved in the modulation of various cellular processes including proliferation, differentiation and apoptosis, making them central to understanding the therapeutic potential of MSC conditioned media [3, 4].

Recent studies have demonstrated that exosomes can mimic the effects of MSC, offering a cell-free therapeutic alternative. For instance, Doeppner *et al.* highlighted the role of exosomes in promoting neuroprotection and neuroregeneration and reducing post-stroke immune responses in a mouse model [5]. Similarly, there is evidence that MSC-derived exosomes enhance wound healing by promoting angiogenesis and cell migration [6, 7]. These results highlight the potential of exosomes as mediators of the therapeutic effects of MSC. In addition, the role of exosomes in cancer biology has been studied, but the results obtained are contradictory — studies have shown both stimulation and suppression of tumor progression by MSC-derived exosomes depending on the type of cancer and the exosomes used [8].

To enhance MSC-CM bioactivity, various enrichment techniques are used, each with distinct advantages and limitations, but more often, enrichment is aimed at increasing the concentration of exosomes [9]. Ultracentrifugation is the most widely used method for exosome enrichment, involving sequential centrifugation to pellet exosomes (100,000–200,000 $\times$ g) [10]. Size-exclusion chromatography (SEC) separates EVs from soluble proteins, however, it may dilute samples [11]. Polymer-based reagents (e.g., polyethylene glycol) precipitate EVs by altering solubility, and commercial kits enable rapid, scalable enrichment but may co-precipitate non-EV components, including lipoproteins [12, 13]. Affinity-based techniques use antibody-coated beads or columns target EV surface markers (e.g., CD9, CD63, CD81) for selective capture [14]. Ultrafiltration uses membranes with specific molecular weight cut-offs (e.g., 10–100 kDa) to concentrate EVs while excluding smaller proteins and can be scaled up for clinical applications [15]. A number of new enrichment approaches employ microfluidic devices that enable label-free, high-throughput isolation of EVs using acoustic, electrophoretic, or immunoaffinity principles. These systems provide rapid processing and minimal sample loss, but require technical expertise [16]. Ultimately, the choice of method largely depends on the goals of the experiment and the requirements for the content of certain biologically active substances in the resulting concentrates.

In this paper, we present post-concentration analysis of enriched MSC-CM fractions obtained after using centrifugal concentrators, which are classified as ultrafiltration devices and may be used for rapid, scalable concentration of MSC-CM components [17]. This method uses molecular weight cut-off (MWCO) membranes to retain the important part of the MSC secretome including EVs. We focus on enriching components of the conditioned medium smaller than 0.2 μm using size-exclusion centrifugal filtration to isolate significant part of proteins and exosomes. To achieve this, the conditioned medium was passed through 80 μm and 0.2 μm syringe filters, followed by centrifugation with 50 and 10 kDa MWCO Amicon® Ultra-15 Centrifugal Filter Units to concentrate the sub-0.2 μm fraction. This enrichment process ensured removal of cellular debris and high molecular weight aggregates and proteins while retaining important bioactive soluble factors, such as cytokines and exosomes, within the target size range. Following enrichment, Western blotting, biolayer interferometry, determination of nanoparticle concentration by ultramicroscopy, scanning and transmission electron microscopy were used to confirm the presence of EVs, including exosomes, in the enriched 0.2 μm–50 kDa fraction. The described approach allows selective concentration of bioactive molecules and exosomes,

which are of crucial importance for subsequent functional application in regenerative medicine, biotechnology, diagnostics and research work. Minimal required equipment and processing time compared to ultracentrifugation or chromatography, suitability for both small-scale research and large-scale production, and preservation of bioactivity with retaining functional EVs and proteins make this high-throughput, easily standardized method perspective for further biotechnological applications, which will enhance the reliability of MSC CM as a cell-free regenerative tool [18].

2. Materials and methods

2.1. Preparation of MSC conditioned media

Cell culture of d293 MSC from adipose tissue was provided by the Collection of cell cultures for biotechnological and biomedical research of the Koltsov Institute of Developmental Biology of RAS. To obtain conditioned medium, MSC were cultured in standard culture medium DMEM (Paneco) supplemented with 10% fetal bovine serum (FBS) (Biowest), alanyl-glutamine and antibiotics (penicillin, streptomycin). MSC (passage five) at concentration $(4.8–5.2) \times 10^6$ were placed on a T175 cultural flask in a DMEM with 10% FBS. After 48–72 h, at 80% cell confluency, the medium was removed, cells were washed twice with phosphate-buffered saline (PBS), and 45 ml DMEM containing 10% FBS or not containing FBS were added. The conditioned medium was collected after 72 h and used for further analysis.

2.2. Filtration and ultrafiltration

Pre-filtration of 15 ml of conditioned media was carried out sequentially through 80 μm filter (Hawach Scientific) and 0.2 μm membrane (polyethylene terephthalate track-etched membranes with pore diameters (0.2 ± 0.01) μm were manufactured at the Flerov Laboratory of Nuclear Reactions, JINR) using reusable syringe filter holder. For ultrafiltration Amicon® Ultra-15 Centrifugal Filter Units with MWCO membranes of 50 and 10 kDa were used at $4000 \times g$ at 25°C.

2.3. Protein and RNA quantification

Protein and RNA concentrations were quantified using the Qubit Fluorometer, Qubit Protein Assay Kit and Qubit RNA High Sensitivity (HS) Assay Kit (Thermo Fisher Scientific) according to the manufacturer's instructions. For three independent conditioned medium samples, three measurements were performed for obtained fractions. Data are presented as mean ± standard deviation (SD).

2.4. Determination of nanoparticle concentration by ultramicroscopy

The concentration of nanoparticles in samples was determined using ultramicroscopy on an NP Counter device (NP VIZHN) according to the manufacturer's instructions. Before measurements, the samples of CM with FBS were diluted 140 times, and the samples of CM without FBS were diluted 15 times. The final content of nanoparticles in the sample was calculated taking into account the dilution.

2.5. Transmission electron microscopy (TEM)

Copper grids with a thin amorphous carbon film (SPI Supplies) were used as the supporting substrate. The grids were pre-treated with UV light for 15 min. Samples were fixed for 30 min with a 2.5% glutaraldehyde solution (25%, Thermo Fisher Scientific) in PBS, adjusted to pH 7 using 0.1 M NaOH (reagent grade, Lenreaktiv), applied onto the grids, and incubated for 10 min. Excess sample was removed, washed with water, dehydrated in a series of acetone (for analysis, PanReac) solutions with concentrations of 10%, 30%, 50%, 70%, 100% for 10 min and stained for 15 s with 2% phosphotungstic acid (reagent grade, Lenreaktiv), adjusted to pH 7 using 0.1 M NaOH. The study using transmission electron microscopy was performed on a Talos F200i S/TEM microscope (Thermo Fisher Scientific) at an accelerating voltage of 200 kV.

2.6. Scanning electron microscopy (SEM)

For samples analysis, silicon wafers were sequentially treated with 35% H_2O_2 (34.5–36.5%, Sigma-Aldrich) for 30 min, followed by rinsing in water for 5 min and isopropanol (99.9%, Sigma-Aldrich) for 5 min. The wafers were then modified with a 1% solution of 3-aminopropyltriethoxysilane (99%, Sigma-Aldrich), adjusted to pH 4 using 0.1 M acetic acid (for analysis, PanReac), at 60°C for 120 min. After modification, the wafers were rinsed with water, isopropanol, and dried at 120°C for 120 min. Samples were fixed with a 2.5% glutaraldehyde solution (25%, Thermo Fisher Scientific), adjusted to pH 7 using 0.1 M NaOH (reagent grade, Lenreaktiv), and applied as a 2 μm layer onto the silicon wafers. The samples were incubated for 10 min, and then washed with water and isopropanol. Scanning electron microscopy was performed using a high-resolution SU 8020 microscope (Hitachi) equipped with a cold field-emission cathode, operating at an accelerating voltage of 3 kV. To enhance surface conductivity, a 5 nm layer of platinum–palladium alloy was sputtered onto the samples using a Q150T S magnetron sputtering system (Quorum). All solutions were prepared with Milli-Q deionized water (Millipore) with a resistivity of 18 M$\Omega \cdot$cm at 22°C.

2.7. Biolayer interferometry

DNA aptamers were synthesized by Synthol (Moscow, Russia): CD63 DNA aptamer 5'-CACCCCACCTCGCTCCCGTGACACTAATGCTA-3'-biotin (biotinylated at the 3' end); SARS-CoV-2 S protein DNA aptamer (control aptamer) biotin-5'-CAGCACCGACCTTGTGCTTTGGGAGTGCTGGTCCAAGGGCGTTAATGGACA-3' (biotinylated at the 5' end). 1 μM aptamer solutions were prepared in PBS, heated at 95°C for 5 min, and cooled to room temperature. Biolayer interferometry (BLI) experiments were performed using a BLItz instrument (ForteBio, Fremont, USA) and streptavidin-coated biosensors (ForteBio, Fremont, USA). Biosensors were hydrated in PBS for 10 min, and biotinylated aptamers were immobilized on the sensors for 3 min. The experimental protocol was as follows: 1) baseline in phosphate-buffered saline for 30 s; 2) samples were allowed to interact with the aptamers for 200 s; 3) dissociation of complexes in PBS for 200 s. Samples were tested in serial dilutions (4×, 10×, and 20×) in PBS. To account for background or nonspecific binding, control aptamer (SARS-CoV-2 S protein) response curves were subtracted from CD63 aptamer response curves.

2.8. Western blot analysis

Exosome-derived protein samples were prepared by combining 100 μL of ice-cold RIPA lysis buffer (10 mM Tris-HCl, pH 8.0, 1 mM EDTA, 0.5 mM EGTA, 1% Triton X-100, 0.1% Sodium

Deoxycholate, 0.1% SDS) supplemented with protease inhibitors with an equal volume of the 0.2 μm–50 kDa CM fraction. The mixture was homogenized by pipetting, incubated on ice for 15 min, and 4× Laemmli Sample Buffer was added. For electrophoresis, 1 (DMEM with 10% FBS), 3 (CM with FBS) or 20 (CM without FBS and DMEM) μL of samples were loaded onto 10% SDS-polyacrylamide gel (BioRad). After separation, proteins were transferred to PVDF membrane (BioRad). Membrane was probed with rabbit polyclonal antibody to Tetraspanin 30 (TSPAN30) recognizing CD63 protein (Cloud-Clone Corp.) at a dilution of 1:1000 for 1 h at room temperature, washed in PBS-0.1%Tween 20 and probed with a goat antirabbit secondary antibody HRP conjugate (Thermo Fisher Scientific) at a dilution of 1:10,000 for 1 h. Chemiluminescent detection was performed using SuperSignal™ West Pico Rabbit IgG Detection Kit (Thermo Fisher Scientific).

3. Results and discussion

3.1. Morphology of used MSC

MSC at passage five are ideal for producing conditioned medium due to the balance between proliferative activity, homogeneity, and minimal senescence of cell culture. Used in our study adipose-derived mesenchymal stem cells at passage five exhibit typical of mesenchymal cells spindle-shaped (fibroblast-like) cell shape with elongated cytoplasmic processes, firmly attached to the culture surface, forming a monolayer with uniform distribution (Figure 1). Cell culture demonstrates morphological purity ($\geq$ 90% of cells display spindle-shaped morphology) and absence of abnormal shapes.

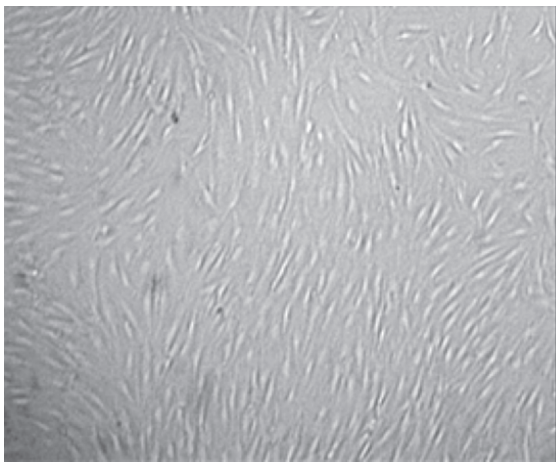

Figure 1. Morphology of adipose-derived MSC exhibited fibroblast-like characteristics.

3.2. Protein and RNA content in conditioned medium fractions

In this paper, we utilized two types of conditioned medium for MSC: obtained using serum-containing culture approach and using serum-free approach. Traditional MSC expansion relies on FBS-supplemented media because FBS provides essential nutrients, adhesion factors, and hormones, ensuring robust cell proliferation and sustained secretory activity. In addition, FBS contains a substantial quantity of EVs ($(2.60 \pm 0.33) \times 10^{10}$ EVs/mL in 10% FBS-supplemented culture medium [19]), including exosomes, which are secreted by bovine cells during serum production. These exosomes may influence MSC by altering their behavior or secretory profiles, and lot-to-lot variability in FBS composition results in inconsistency in the composition of

the conditioned medium [20]. Ethical concerns and risks of xenogeneic pathogen transfer also limit its suitability for clinical applications. Serum-free media contains basic nutrients for cellular metabolism and proliferation and eliminates animal-derived components, reduces immunogenicity risks, enhances reproducibility, and aligns with regulatory standards for clinical-grade MSC products. It also avoids confounding effects of serum proteins in downstream analyses [19]. However, this approach possibly reduces secretory output compared to serum-rich environments. Thus, the choice of approach to obtaining MSC conditioned medium depends on the final goals, and we present data on the total protein and RNA content of fractions of serum-containing and serum-free conditioned medium to better guide this choice (Table 1, Table 2).

DMEM we used contains about 950 mg/l of amino acids that are essential for maintaining cellular metabolism in cultured cells, including glycine (30 mg/l), which can slightly affect measurements of protein concentration with the Qubit Protein BR Assay. Therefore, the values

Table 1. Quantification of total protein in different fractions generated by filtration and ultrafiltration of MSC conditioned serum-containing and serum-free medium. Serum-free DMEM was used as a control for the initial protein content. Data are presented as mean ± SD. CM — conditioned medium. NM — not measured.

	DMEM	DMEM with 10% FBS	CM without FBS	CM with 10% FBS
	Protein (mg/ml)			
Before filtration	0.034	4.010 ± 0.48	0.044 ± 0.0006	4.080 ± 0.69
After 80 μm filter	NM	NM	NM	3.530 ± 0.43
Fraction 0.2 μm–50 kDa, reduction of the initial sample volume $\sim$ 15 times	0.032 ± 0.0006	11.23 ± 0.83	0.150 ± 0.02	2.410 ± 0.036
Fraction 50–10 kDa, reduction of the initial sample volume $\sim$ 40 times	0.031 ± 0.0006	0.077 ± 0.003	0.032 ± 0.0002	1.670 ± 0.46
Fraction $<$ 10 kDa	0.032 ± 0.0006	0.029 ± 0.0032	0.031 ± 0.0006	0.200 ± 0.0001

Table 2. Quantification of non-vesicular RNA in different fractions generated by filtration and ultrafiltration of MSC conditioned serum-containing and serum-free medium. Serum-free DMEM was used as a control for the initial RNA content. Data are presented as mean ± SD. CM — conditioned medium. TL — too low, concentrations below detection limit. NM — not measured.

	DMEM	CM without FBS	CM with 10% FBS
	RNA (ng/μl)		
Before filtration	TL	TL	16.86 ± 3.40
After 80 μm filter	NM	NM	12.13 ± 0.53
Fraction 0.2 μm–50 kDa, reduction of the initial sample volume $\sim$ 15 times	TL	TL	109.13 ± 6.99
Fraction 50–10 kDa, reduction of the initial sample volume $\sim$ 40 times	TL	TL	TL
Fraction $<$ 10 kDa	TL	TL	TL

obtained for protein concentrations measured in DMEM (Table 1) can be attributed to the effect of glycine, other primary amines or phenol red and can be considered as background values. Addition of 10% FBS to DMEM increased the protein concentration by more than 100-fold (4.010 mg/mL vs. 0.034 mg/mL).

In the serum-free conditioned medium, all studied fractions showed protein content values corresponding to background values, with the exception of fraction 0.2 μm–50 kDa where the protein content was $\sim$ 0.15 mg/ml. This fraction contains the bulk of the MSC secretome with proteins approximately less than 2000 kDa [21] and EVs with a diameter less than 200 nm, including exosomes. In contrast, the medium with 10% FBS contained proteins in all fractions analyzed, and most of the proteins were filtered by the 0.2 μm filter. It can be assumed that the main part of the MSC secretome in the conditioned medium with FBS is also in the 0.2 μm–50 kDa fraction, however, a significant part of this fraction most likely consists of proteins and EVs of serum origin.

In addition to proteins, FBS contains diverse RNA species, including mRNAs, miRNAs, and long non-coding RNAs, primarily encapsulated within extracellular vesicles like exosomes or bound to carrier proteins [22]. These bovine cell-derived RNA molecules can be transferred into cultured MSC, potentially influencing gene expression and secretory outcomes [23]. According to our measurements, CM with FBS contains a significant amount of non-vesicular RNA (free-floating or protein-bound), and the maximum content of such RNA is observed in the concentrated 0.2 μm–50 kDa fraction. In contrast, no fraction of the conditioned medium without FBS and initial DMEM contained non-vesicular RNA (Table 2).

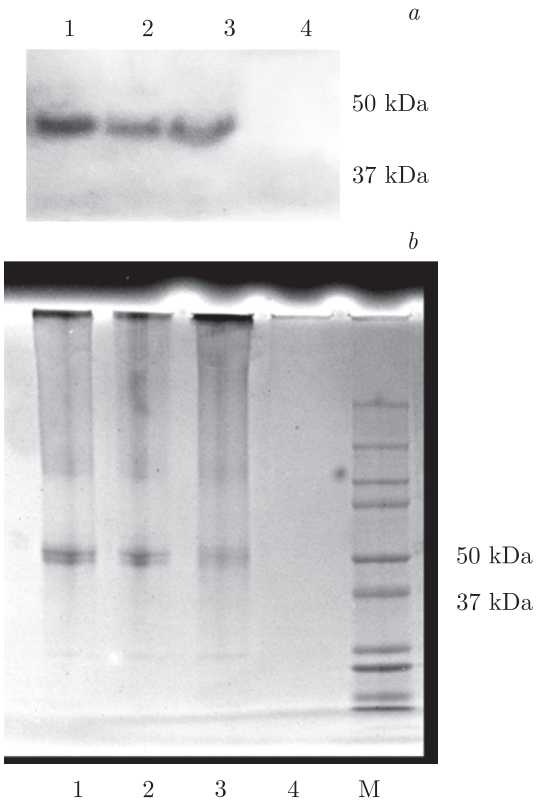

Figure 2. Western blot analysis using anti-CD63 antibody (*a*) and SDS-PAGE (*b*) of the 0.2 μm–50 kDa fraction of serum-containing CM (1), serum-free CM (2), DMEM+10% FBS (3), and DMEM (4). M — Precision Plus Protein Dual Color Standards (BioRad). To load a comparable total mass of protein per lane, the volumes of samples loaded are related as follows: 3:20:1:20.

In addition, we did a Western blot with anti-CD63 antibody for the 0.2μm–50 kDa fractions. CD63, a tetraspanin protein enriched in exosomal membranes, is widely used as a biomarker to confirm presence of exosomes [24]. We observe a strong CD63 signal in Western blotting for the 0.2 μm–50 kDa fraction of DMEM+10% FBS and CM with FBS, indicating a high content of exosomes in these fractions, and absence of signal for the 0.2 μm–50 kDa fraction of DMEM (Figure 2). The binding of used anti-CD63 antibodies to both MSC-derived CD63 proteins and FBS-derived CD63 proteins is likely a result of the extremely high homology (up to 95%) between the specific epitopes of human and bovine CD63 [23].

The CD63 signal for the 0.2 μm–50 kDa fraction of serum-free CM is also present, and its intensity is lower than for the same fraction of CM with FBS. This difference in CD63 signal intensity may reflect the contribution of FBS-derived exosomes to the CD63 pool in serum-containing CM and/or reduced exosome secretion by cells cultured in serum-free conditions. However, the presence of the CD63 signal in the 0.2 μm–50 kDa fraction of serum-free CM indicates that MSC secrete exosomes even in the absence of FBS and the selected fraction in both variants of obtaining the conditioned medium contain exosomes that can be used for further application.

3.3. Nanoparticle concentration in CM and 0.2 μm–50 kDa CM fraction

The concentration of suspended nanoparticles, including exosomes, in CM with 10% FBS, without FBS and their 0.2 μm–50 kDa fractions were quantitatively assessed using ultramicroscopy, a method offering for nanoparticle detection [25] (Table 3).

Table 3. Concentration of suspended nanoparticles in CM with 10% FBS, without FBS and their 0.2 μm–50 kDa fractions obtained by ultramicroscopy. Data are presented as mean ± SD. CM — conditioned medium.

Sample	Concentration (pcs/ml)
DMEM with 10% FBS	$(6.7 \pm 2.98) \times 10^{11}$
DMEM with 10% FBS, fraction 0.2 μm–50 kDa, reduction of the initial sample volume ∼ 15 times	$(3 \pm 0.36) \times 10^{12}$
CM with 10% FBS	$(9.7 \pm 2.8) \times 10^{11}$
CM with 10% FBS, fraction 0.2 μm–50 kDa, reduction of the initial sample volume ∼ 15 times	$(1.4 \pm 0.28) \times 10^{12}$
CM without FBS	$(4.8 \pm 2.2) \times 10^{10}$
CM without FBS, fraction 0.2 μm–50 kDa, reduction of the initial sample volume ∼ 15 times	$(5.7 \pm 2.7) \times 10^{10}$

DMEM medium with 10% FBS exhibits high levels of particles (including EVs, lipoproteins and protein aggregates), clearly demonstrating the overwhelming contribution of FBS to particle numbers in standard FBS-supplemented media. According to measurements, particle concentration in FBS-containing CM is an order of magnitude higher than in FBS-free CM. The 0.2 μm–50 kDa fraction of FBS-containing CM retains high particle counts, however, nanoparticles concentration increased by ∼ 1.4-fold, which is below the expected 15-fold increase. This can be explained by adsorption of large EVs and protein aggregates on the 0.2 μm

filter during ultrafiltration, i.e. most particles in the FBS-containing CM are outside the 0.2 μm–50 kDa range. After fractionation, CM without FBS contains $\sim$ 40-fold fewer particles than fractionated CM with FBS (5.7×10^{10} vs. 1.4×10^{12}). This highlights the dominant role of FBS in particle pool formation, potentially masking MSC-specific vesicles or proteins in serum-containing media and confirming the critical role of FBS in nanoparticle accumulation. Considering that FBS contains a significant amount of bovine EVs ($(2.60 \pm 0.33) \times 10^{10}$ EVs/mL in 10% culture medium supplemented with FBS [19]), it can be concluded that a portion of nanoparticles in the FBS-containing CM represents bovine-derived EVs, which will complicate the isolation and analysis of MSC-derived EVs (e.g., exosomes).

3.4. TEM and SEM of conditioned medium of fractions 0.2 μm–50 kDa

To confirm the presence of extracellular vesicles in the studied samples, we obtained TEM and SEM images, which can serve as evidence for the presence of EVs by confirming their characteristic size and morphology [26].

TEM and SEM images of CM with 10% FBS fraction 0.2 μm–50 kDa (Figure 3, *a*, 3, *c*) revealed particles with a size of 50–150 nm, which is consistent with the expected size range for EVs [27], but in the case of SEM, definitive identification of EVs was hindered by the high protein content and serum-derived contaminants make it difficult to distinguish between EVs and non-vesicular particles. TEM and SEM images of the serum-free CM 0.2 μm–50 kDa

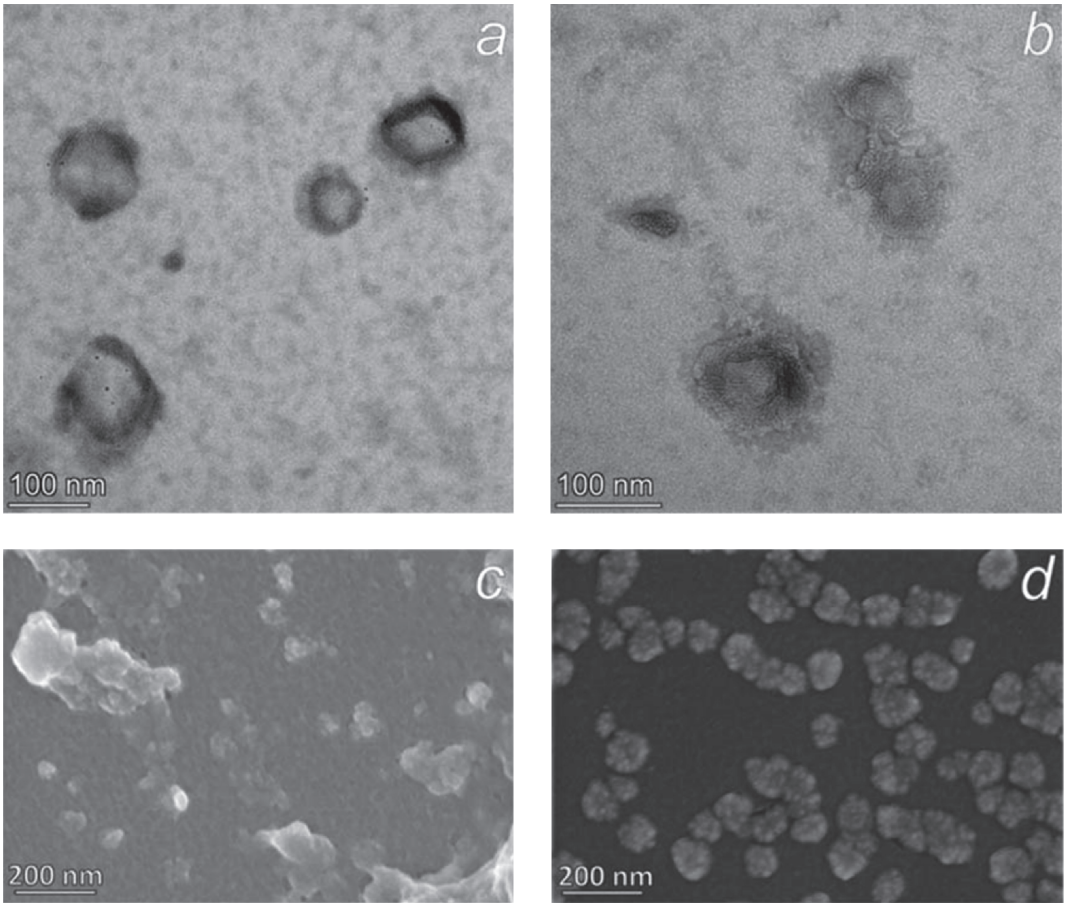

Figure 3. Electron microscopy of CM 0.2 μm–50 kDa fraction samples: *a*) TEM CM with 10% FBS, fraction 0.2 μm–50 kDa; *b*) TEM CM without FBS, fraction 0.2 μm–50 kDa; *c*) SEM CM with 10% FBS, fraction 0.2 μm–50 kDa; *d*) SEM CM without FBS, fraction 0.2 μm–50 kDa.

fraction (Figure 3, *b*, 3, *d*) revealed vesicle-like structures consistent with the size and cup-shaped morphology typical of extracellular vesicles, supporting their presence in the sample [28].

3.5. Biolayer interferometry results

In addition, the presence of exosomes in the samples was proved by biolayer interferometry, a method for determining the affinity of biomolecules using minimal sample volumes (from 4 μl per experiment). The CD63-2 sequence proposed by Song *et al.* was chosen as the DNA aptamer [29] to the exosome-specific marker CD63 [30], which, after a slight modification, was successfully used within several sensors [31–35]. The DNA aptamer was synthesized with a biotin modification that allowed the aptamer to be immobilized on a streptavidin sensor. Association and dissociation curves for exosomes interacting with DNA aptamers on a sensor are shown in Figure 4.

The intensity of the interference shift is proportional to the amount of adsorbed matter on the sensor. According to biolayer interferometry results, all studied samples contained exosomes, however, the largest number of CD63-positive exosomes was found in the serum-

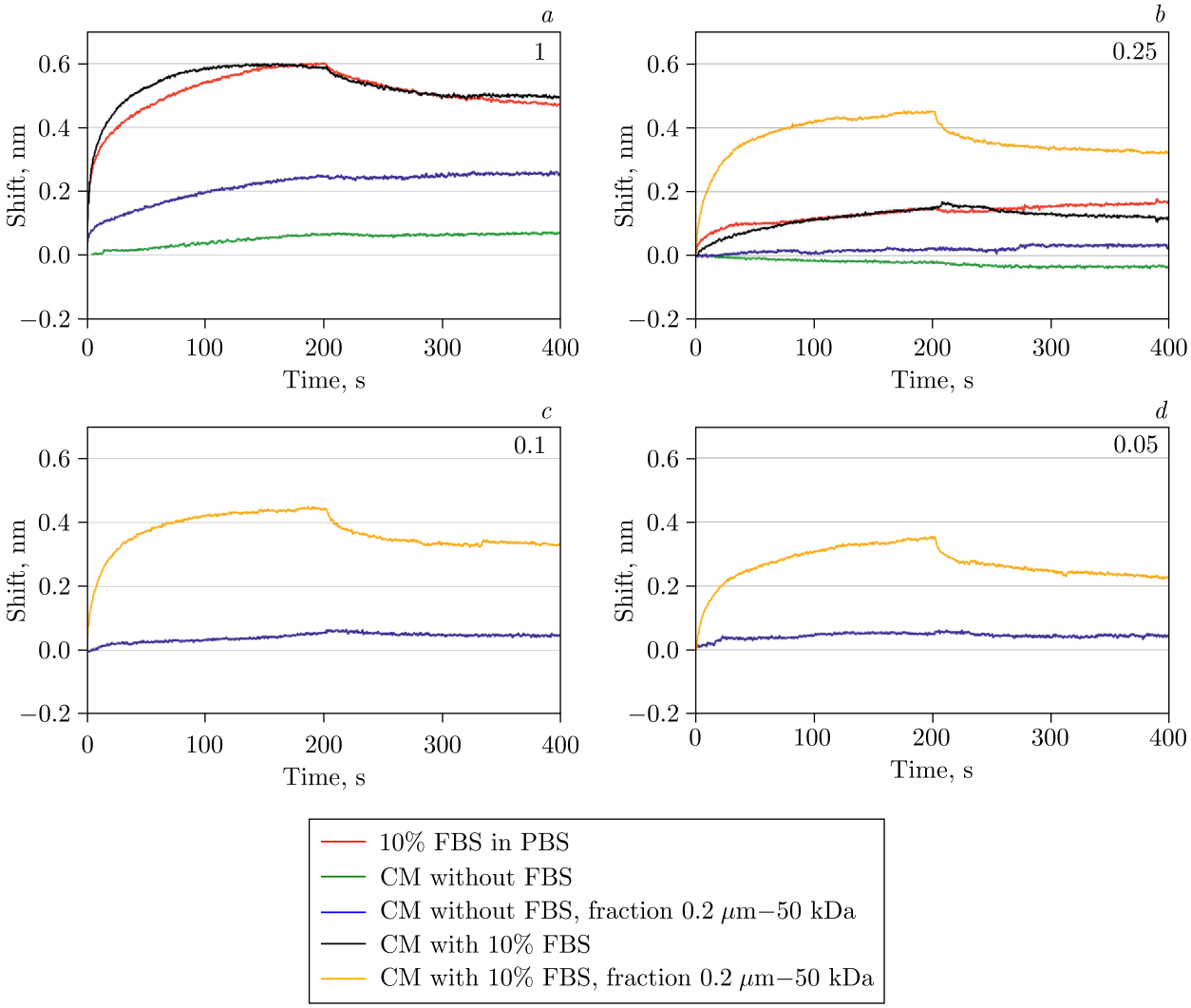

Figure 4. Biolayer interferometry sensorgrams for determination of the exosomes presence for: *a*) 1 — samples without dilution; *b*) 0.25 — the original samples diluted 4 times; *c*) 0.1 — the original samples diluted 10 times; *d*) 0.05 — the original samples diluted 20 times.

containing CM samples, which most likely reflects elevated exosome secretion rates and the contribution of residual FBS-derived exosomes. As a control, experiments were conducted on the interaction of the CD63 aptamer with 10% FBS solution (Figure 4) containing bovine exosomes. Indeed, intense binding of the aptamer to the FBS components was observed. The control experiment with 10% FBS solution demonstrates that the used CD63 aptamer cross-reacts with bovine exosomes present in FBS and the assay detects both human and bovine exosomes due to similar CD63 epitopes. Thus, serum-containing CM samples are likely to contain a mixed population of human and bovine exosomes, complicating the interpretation of exosome quantification as the assay cannot differentiate between endogenous (human) and exogenous (FBS-derived) exosomes.

4. Conclusion

In this paper, we compare the composition of two types of MSC CM obtained using serum-containing and serum-free culture approaches and reveal differences in composition and concentration of CM components. Total protein, non-vesicular RNA, exosome and nanoparticle levels in serum-containing CM fractions are markedly higher than in serum-free CM, reflecting both MSC-derived components and residual FBS contribution in serum-containing CM, making them suitable for applications where yield outweighs purity concerns (e.g., preliminary biomarker discovery). In contrast, serum-free CM fractions exhibit lower protein/RNA/exposome/nanoparticle content but provide a "purer" profile of the MSC-derived secretome, which is critical for therapeutic purposes where regulatory compliance may require the exclusion of animal-derived components. In addition, we demonstrate that the 0.2 μm–50 kDa fraction of CM obtained with ultrafiltration and enriched in exosomes and proteins makes up a significant part of the MSC secretome. This fractionation strategy allows the isolation of small vesicles and mid-sized proteins excluding larger and smaller components, while exosomes and a significant portion of the functionally important proteins of the MSC secretome are retained in this fraction in higher concentrations than in the original CM. Further, the entire filtration process can be carried out using polyethylene terephthalate track-etched membranes, which have a number of advantages: cylindrical pores with near-identical diameters (±5–10% variance), good mechanical and thermal stability, biocompatibility [36, 37], which makes them suitable for GMP implementation and filtration scaling.

It should be noted that a clear assessment of the amount of FBS components consumed by cells and MSC-secreted substances in resulted FBS-containing CM is a difficult task. The complex composition of FBS, which includes proteins and EVs, overlaps with MSC-secreted biomolecules, making it difficult to distinguish between consumed serum components and newly released cellular products. High-abundance FBS proteins (e.g., albumin and fibronectin) often dominate analytical assays, masking low-concentration MSC-derived factors. Dynamic changes in FBS component stability, such as degradation of its components over time, complicate efforts to quantify what is truly consumed versus passively degrade in the conditioned medium. Metabolic labeling (e.g., SILAC) of cellular proteins could theoretically separate newly synthesized MSC-derived components of medium from pre-existing components [38], but at the moment it is difficult to bypass all the methodological limitations necessary to conduct such an experiment in serum-containing systems. Nevertheless, advances in synthetic media development and scaffold generation technologies may narrow the functional gap between serum-containing and serum-free methods of MSC cultivation, enabling the production of customized MSC culture media for a variety of biomedical applications.

Acknowledgements

The authors are grateful to Nikolay Lizunov and Oleg Orelovich for the help with SEM examination of samples, Alisher Mutali for the help with TEM examination of samples and Kirill Tarasov for the data visualization.

Author contributions

E. Andreev: Data curation, Writing, Original draft preparation, Visualization, Investigation; E. Kravchenko: Data curation, Writing, Original draft preparation, Investigation, Supervision, Validation, Reviewing and Editing; E. Zavyalova: Data curation, Writing, Original draft preparation, Visualization, Investigation; P. Eremin: Data curation, Original draft preparation, Methodology; A. Rzyanina: Data curation, Original draft preparation, Visualization; P. Markov: Original draft preparation, Methodology; A. Nechaev: Conceptualization, Methodology, Supervision, Validation.

Funding

The research was funded by the Joint Institute for Nuclear Research within the framework of projects Nanocomposite and functional track membranes 07-5-1131-2-2024/2028, Highly sensitive sensors operating on the principles of molecular recognition for virus detection 07-5-1131-3-2025/2029, TARDISS 05-2-1132-1-2021/2028.

Conficts of interest

The authors declare no conflicts of interest.

References

[1] Y. Seo, T. H. Shin, H. S. Kim, Current strategies to enhance adipose stem cell function: An update, Int. J. Mol. Sci. (2019). https://doi.org/10.3390/ijms20153827.

[2] A. González-González, D. García-Sánchez, M. Dotta, J. C. Rodríguez-Rey, F. M. Pérez-Campo, Mesenchymal stem cells secretome: The cornerstone of cell-free regenerative medicine, World J. Stem Cells (2020). https://doi.org/10.4252/wjsc.v12.i12.1529.

[3] X. L. Fan, Y. Zhang, X. Li, Q. L. Fu, Mechanisms underlying the protective effects of mesenchymal stem cell-based therapy, Cell. Mol. Life Sci. (2020). https://doi.org/10.1007/s00018-020-03454-6.

[4] G. Yang, X. Fan, Y. Liu, P. Jie, M. Mazhar, Y. Liu, N. Dechsupa, L. Wang, Immunomodulatory mechanisms and therapeutic potential of mesenchymal stem cells, Stem Cell Rev. Rep. (2023). https://doi.org/10.1007/s12015-023-10539-9.

[5] T. R. Doeppner, J. Herz, A. Görgens, J. Schlechter, A.-K. Ludwig, S. Radtke, K. de Miroschedji, P. A. Horn, B. Giebel, D. M. Hermann, Extracellular vesicles improve post-stroke neuroregeneration and prevent postischemic immunosuppression, Stem Cells Transl. Med. (2015). https://doi.org/10.5966/sctm.2015-0078.

[6] R. Tutuianu, A. M. Rosca, D. M. Iacomi, M. Simionescu, I. Titorencu, Human mesenchymal stromal cell-derived exosomes promote *in vitro* wound healing by modulating the biological properties of skin keratinocytes and fibroblasts and stimulating angiogenesis, Int. J. Mol. Sci. (2021). https://doi.org/10.3390/ijms22126239.

[7] A. Shabbir, A. Cox, L. Rodriguez-Menocal, M. Salgado, E. Van Badiavas, Mesenchymal stem cell exosomes induce proliferation and migration of normal and chronic wound fibroblasts, and enhance angiogenesis *in vitro*, Stem Cells Dev. (2015). https://doi.org/10.1089/scd.2014.0316.

[8] Y. Slama, F. Ah-Pine, M. Khettab, A. Arcambal, M. Begue, F. Dutheil, P. Gasque, The dual role of mesenchymal stem cells in cancer pathophysiology: Pro-tumorigenic effects versus therapeutic potential, Int. J. Mol. Sci. (2023). https://doi.org/10.3390/ijms241713511.

[9] C. Théry, K. W. Witwer, E. Aikawa, M. J. Alcaraz, J. D. Anderson, R. Andriantsitohaina, A. Antoniou, T. Arab, F. Archer, G. K. Atkin-Smith, D. C. Ayre, J. M. Bach, D. Bachurski, H. Baharvand, L. Balaj, S. Baldacchino, N. N. Bauer, A. A. Baxter, M. Bebawy, C. Beckham, A. Bedina Zavec, A. Benmoussa, A. C. Berardi, P. Bergese, E. Bielska, C. Blenkiron, S. Bobis-Wozowicz, E. Boilard, W. Boireau, A. Bongiovanni, F. E. Borràs, S. Bosch, C. M. Boulanger, X. Breakefield, A. M. Breglio, M. Brennan, D. R. Brigstock, A. Brisson, M. L. D. Broekman, J. F. Bromberg, P. Bryl-Górecka, S. Buch, A. H. Buck, D. Burger, S. Busatto, D. Buschmann, B. Bussolati, E. I. Buzás, J. B. Byrd, G. Camussi, D. R. F. Carter, S. Caruso, L. W. Chamley, Y. T. Chang, A. D. Chaudhuri, C. Chen, S. Chen, L. Cheng, A. R. Chin, A. Clayton, S. P. Clerici, A. Cocks, E. Cocucci, R. J. Coffey, A. Cordeiro-da-Silva, Y. Couch, F. A. W. Coumans, B. Coyle, R. Crescitelli, M. F. Criado, C. D'Souza-Schorey, S. Das, P. de Candia, E. F. De Santana, O. De Wever, H. A. del Portillo, T. Demaret, S. Deville, A. Devitt, B. Dhondt, D. Di Vizio, L. C. Dieterich, V. Dolo, A. P. Dominguez Rubio, M. Dominici, M. R. Dourado, T. A. P. Driedonks, F. V. Duarte, H. M. Duncan, R. M. Eichenberger, K. Ekström, S. El Andaloussi, C. Elie-Caille, U. Erdbrügger, J. M. Falcón-Pérez, F. Fatima, J. E. Fish, M. Flores-Bellver, A. Försönits, A. Frelet-Barrand, F. Fricke, G. Fuhrmann, S. Gabrielsson, A. Gámez-Valero, C. Gardiner, K. Gärtner, R. Gaudin, Y. S. Gho, B. Giebel, C. Gilbert, M. Gimona, I. Giusti, D. C. I. Goberdhan, A. Görgens, S. M. Gorski, D. W. Greening, J. C. Gross, A. Gualerzi, G. N. Gupta, D. Gustafson, A. Handberg, R. A. Haraszti, P. Harrison, H. Hegyesi, A. Hendrix, A. F. Hill, F. H. Hochberg, K. F. Hoffmann, B. Holder, H. Holthofer, B. Hosseinkhani, G. Hu, Y. Huang, V. Huber, S. Hunt, A. G. E. Ibrahim, T. Ikezu, J. M. Inal, M. Isin, A. Ivanova, H. K. Jackson, S. Jacobsen, S. M. Jay, M. Jayachandran, G. Jenster, L. Jiang, S. M. Johnson, J. C. Jones, A. Jong, T. Jovanovic-Talisman, S. Jung, R. Kalluri, S. ichi Kano, S. Kaur, Y. Kawamura, E. T. Keller, D. Khamari, E. Khomyakova, A. Khvorova, P. Kierulf, K. P. Kim, T. Kislinger, M. Klingeborn, D. J. Klinke, M. Kornek, M. M. Kosanović, Á. F. Kovács, E. M. Krämer-Albers, S. Krasemann, M. Krause, I. V. Kurochkin, G. D. Kusuma, S. Kuypers, S. Laitinen, S. M. Langevin, L. R. Languino, J. Lannigan, C. Lässer, L. C. Laurent, G. Lavieu, E. Lázaro-Ibáñez, S. Le Lay, M. S. Lee, Y. X. F. Lee, D. S. Lemos, M. Lenassi, A. Leszczynska, I. T. S. Li, K. Liao, S. F. Libregts, E. Ligeti, R. Lim, S. K. Lim, A. Linē, K. Linnemannstöns, A. Llorente, C. A. Lombard, M. J. Lorenowicz, Á. M. Lörincz, J. Lötvall, J. Lovett, M. C. Lowry, X. Loyer, Q. Lu, B. Lukomska, T. R. Lunavat, S. L. N. Maas, H. Malhi, A. Marcilla, J. Mariani, J. Mariscal, E. S. Martens-Uzunova, L. Martin-Jaular, M. C. Martinez, V. R. Martins, M. Mathieu, S. Mathivanan, M. Maugeri, L. K. McGinnis, M. J. McVey, D. G. Meckes, K. L. Meehan, I. Mertens, V. R. Minciacchi, A. Möller, M. Møller Jørgensen, A. Morales-Kastresana, J. Morhayim, F. Mullier, M. Muraca, L. Musante, V. Mussack, D. C. Muth, K. H. Myburgh, T. Najrana, M. Nawaz, I. Nazarenko, P. Nejsum, C. Neri, T. Neri, R. Nieuwland, L. Nimrichter, J. P. Nolan, E. N. M. Nolte-'t Hoen, N. Noren Hooten, L. O'Driscoll, T. O'Grady, A. O'Loghlen, T. Ochiya, M. Olivier, A. Ortiz, L. A. Ortiz, X. Osteikoetxea, O. Ostegaard, M. Ostrowski, J. Park, D. M. Pegtel, H. Peinado, F. Perut, M. W. Pfaffl, D. G. Phinney, B. C. H. Pieters, R. C. Pink, D. S. Pisetsky, E. Pogge von Strandmann, I. Polakovicova, I. K. H. Poon, B. H. Powell, I. Prada, L. Pulliam, P. Quesenberry, A. Radeghieri, R. L. Raffai, S. Raimondo, J. Rak, M. I. Ramirez, G. Raposo, M. S. Rayyan, N. Regev-Rudzki, F. L. Ricklefs, P. D. Robbins, D. D. Roberts, S. C. Rodrigues, E. Rohde, S. Rome, K. M. A. Rouschop, A. Rughetti, A. E. Russell, P. Saá, S. Sahoo, E. Salas-Huenuleo, C. Sánchez, J. A. Saugstad, M. J. Saul, R. M. Schiffelers, R. Schneider, T. H. Schøyen, A. Scott, E. Shahaj, S. Sharma,

O. Shatnyeva, F. Shekari, G. V. Shelke, A. K. Shetty, K. Shiba, P. R. M. Siljander, A. M. Silva, A. Skowronek, O. L. Snyder, R. P. Soares, B. W. Sódar, C. Soekmadji, J. Sotillo, P. D. Stahl, W. Stoorvogel, S. L. Stott, E. F. Strasser, S. Swift, H. Tahara, M. Tewari, K. Timms, S. Tiwari, R. Tixeira, M. Tkach, W. S. Toh, R. Tomasini, A. C. Torrecilhas, J. P. Tosar, V. Toxavidis, L. Urbanelli, P. Vader, B. W. M. van Balkom, S. G. van der Grein, J. Van Deun, M. J. C. van Herwijnen, K. Van Keuren-Jensen, G. van Niel, M. E. van Royen, A. J. van Wijnen, M. H. Vasconcelos, I. J. Vechetti, T. D. Veit, L. J. Vella, É. Velot, F. J. Verweij, B. Vestad, J. L. Viñas, T. Visnovitz, K. V. Vukman, J. Wahlgren, D. C. Watson, M. H. M. Wauben, A. Weaver, J. P. Webber, V. Weber, A. M. Wehman, D. J. Weiss, J. A. Welsh, S. Wendt, A. M. Wheelock, Z. Wiener, L. Witte, J. Wolfram, A. Xagorari, P. Xander, J. Xu, X. Yan, M. Yáñez-Mó, H. Yin, Y. Yuana, V. Zappulli, J. Zarubova, V. Žėkas, J. Ye Zhang, Z. Zhao, L. Zheng, A. R. Zheutlin, A. M. Zickler, P. Zimmermann, A. M. Zivkovic, D. Zocco, E. K. Zuba-Surma, Minimal information for studies of extracellular vesicles 2018 (MISEV2018): A position statement of the International Society for Extracellular Vesicles and update of the MISEV2014 guidelines, J. Extracell. Vesicles (2018). https://doi.org/10.1080/20013078.2018.1535750.

[10] C. Gardiner, D. Di Vizio, S. Sahoo, C. Théry, K. W. Witwer, M. Wauben, A. F. Hill, Techniques used for the isolation and characterization of extracellular vesicles: Results of a worldwide survey, J. Extracell. Vesicles (2016). https://doi.org/10.3402/jev.v5.32945.

[11] A. N. Böing, E. van der Pol, A. E. Grootemaat, F. A. W. Coumans, A. Sturk, R. Nieuwland, Single-step isolation of extracellular vesicles by size-exclusion chromatography, J. Extracell. Vesicles (2014). https://doi.org/10.3402/jev.v3.23430.

[12] N. García-Romero, R. Madurga, G. Rackov, I. Palacín-Aliana, R. Núñez-Torres, A. Asensi-Puig, J. Carrión-Navarro, S. Esteban-Rubio, H. Peinado, A. González-Neira, V. González-Rumayor, C. Belda-Iniesta, A. Ayuso-Sacido, Polyethylene glycol improves current methods for circulating extracellular vesicle-derived DNA isolation, J. Transl. Med. (2019). https://doi.org/10.1186/s12967-019-1825-3.

[13] E. Serrano-Pertierra, M. Oliveira-Rodríguez, M. Rivas, P. Oliva, J. Villafani, A. Navarro, M. C. Blanco-López, E. Cernuda-Morollón, Characterization of plasma-derived extracellular vesicles isolated by different methods: A comparison study, Bioengineering (2019). https://doi.org/10.3390/bioengineering6010008.

[14] B. J. Tauro, D. W. Greening, R. A. Mathias, H. Ji, S. Mathivanan, A. M. Scott, R. J. Simpson, Comparison of ultracentrifugation, density gradient separation, and immunoaffinity capture methods for isolating human colon cancer cell line LIM1863-derived exosomes, Methods (2012). https://doi.org/10.1016/j.ymeth.2012.01.002.

[15] M. Y. Konoshenko, E. A. Lekchnov, A. V. Vlassov, P. P. Laktionov, Isolation of extracellular vesicles: General methodologies and latest trends, BioMed Res. Int. (2018). https://doi.org/10.1155/2018/8545347.

[16] Y. Zhang, J. Bi, J. Huang, Y. Tang, S. Du, P. Li, Exosome: A review of its classification, isolation techniques, storage, diagnostic and targeted therapy applications, Int. J. Nanomed. (2020). https://doi.org/10.2147/IJN.S264498.

[17] R. Skovronova, E. Scaccia, S. Calcat-i-Cervera, B. Bussolati, T. O'Brien, K. Bieback, Adipose stromal cells bioproducts as cell-free therapies: Manufacturing and therapeutic dose determine *in vitro* functionality, J. Transl. Med. (2023). https://doi.org/10.1186/s12967-023-04602-9.

[18] T. Lener, M. Gimona, L. Aigner, V. Börger, E. Buzas, G. Camussi, N. Chaput, D. Chatterjee, F. A. Court, H. A. del Portillo, L. O'Driscoll, S. Fais, J. M. Falcon-Perez, U. Felderhoff-Mueser, L. Fraile, Y. S. Gho, A. Görgens, R. C. Gupta, A. Hendrix, D. M. Hermann, A. F. Hill, F. Hochberg, P. A. Horn, D. de Kleijn, L. Kordelas, B. W. Kramer, E. M. Krämer-Albers, S. Laner-Plamberger, S. Laitinen, T. Leonardi, M. J. Lorenowicz, S. K. Lim, J. Lötvall, C. A. Maguire, A. Marcilla, I. Nazarenko, T. Ochiya, T. Patel, S. Pedersen, G. Pocsfalvi, S. Pluchino, P. Que-

senberry, I. G. Reischl, F. J. Rivera, R. Sanzenbacher, K. Schallmoser, I. Slaper-Cortenbach, D. Strunk, T. Tonn, P. Vader, B. W. M. van Balkom, M. Wauben, S. El Andaloussi, C. Théry, E. Rohde, B. Giebel, Applying extracellular vesicles based therapeutics in clinical trials — An ISEV position paper, J. Extracell. Vesicles (2015). https://doi.org/10.3402/jev.v4.30087.

[19] B. M. Lehrich, Y. Liang, P. Khosravi, H. J. Federoff, M. S. Fiandaca, Fetal bovine serum-derived extracellular vesicles persist within vesicle-depleted culture media, Int. J. Mol. Sci. (2018). https://doi.org/10.3390/ijms19113538.

[20] B. M. Lehrich, Y. Liang, M. S. Fiandaca, Foetal bovine serum influence on *in vitro* extracellular vesicle analyses, J. Extracell. Vesicles (2021). https://doi.org/10.1002/jev2.12061.

[21] H. P. Erickson, Size and shape of protein molecules at the nanometer level determined by sedimentation, gel filtration, and electron microscopy, Biol. Proced. Online (2009). https://doi.org/10.1007/s12575-009-9008-x.

[22] Z. Wei, A. O. Batagov, D. R. F. Carter, A. M. Krichevsky, Fetal bovine serum RNA interferes with the cell culture derived extracellular RNA, Sci. Rep. (2016). https://doi.org/10.1038/srep31175.

[23] G. V. Shelke, C. Lässer, Y. S. Gho, J. Lötvall, Importance of exosome depletion protocols to eliminate functional and RNA-containing extracellular vesicles from fetal bovine serum, J. Extracell. Vesicles (2014). https://doi.org/10.3402/jev.v3.24783.

[24] B. S. Joshi, M. A. de Beer, B. N. G. Giepmans, I. S. Zuhorn, Endocytosis of extracellular vesicles and release of their cargo from endosomes, ACS Nano (2020). https://doi.org/10.1021/acsnano.9b10033.

[25] J. Wei, T. Qi, C. Hao, S. Zong, Z. Wang, Y. Cui, Optical microscopic and spectroscopic detection of exosomes, TrAC — Trends Anal. Chem. (2023). https://doi.org/10.1016/j.trac.2023.117077.

[26] J. Lötvall, A. F. Hill, F. Hochberg, E. I. Buzás, D. Di Vizio, C. Gardiner, Y. S. Gho, I. V. Kurochkin, S. Mathivanan, P. Quesenberry, S. Sahoo, H. Tahara, M. H. Wauben, K. W. Witwer, C. Théry, Minimal experimental requirements for definition of extracellular vesicles and their functions: A position statement from the International Society for Extracellular Vesicles, J. Extracell. Vesicles (2014). https://doi.org/10.3402/jev.v3.26913.

[27] M. Colombo, G. Raposo, C. Théry, Biogenesis, secretion, and intercellular interactions of exosomes and other extracellular vesicles, Annu. Rev. Cell Dev. Biol. (2014). https://doi.org/10.1146/annurev-cellbio-101512-122326.

[28] M. Malenica, M. Vukomanović, M. Kurtjak, V. Masciotti, S. Dal Zilio, S. Greco, M. Lazzarino, V. Krušić, M. Perčić, I. J. Badovinac, K. Wechtersbach, I. Vidović, V. Baričević, S. Valić, P. Lučin, N. Kojc, K. Grabušić, Perspectives of microscopy methods for morphology characterisation of extracellular vesicles from human biofluids, Biomedicines (2021). https://doi.org/10.3390/biomedicines9060603.

[29] Z. Song, J. Mao, R. A. Barrero, P. Wang, F. Zhang, T. Wang, Development of a CD63 aptamer for efficient cancer immunochemistry and immunoaffinity-based exosome isolation, Molecules (2020). https://doi.org/10.3390/molecules25235585.

[30] M. Mathieu, N. Névo, M. Jouve, J. I. Valenzuela, M. Maurin, F. J. Verweij, R. Palmulli, D. Lankar, F. Dingli, D. Loew, E. Rubinstein, G. Boncompain, F. Perez, C. Théry, Specificities of exosome versus small ectosome secretion revealed by live intracellular tracking of CD63 and CD9, Nat. Commun. (2021). https://doi.org/10.1038/s41467-021-24384-2.

[31] X. Yu, L. He, M. Pentok, H. Yang, Y. Yang, Z. Li, N. He, Y. Deng, S. Li, T. Liu, X. Chen, H. Luo, An aptamer-based new method for competitive fluorescence detection of exosomes, Nanoscale (2019). https://doi.org/10.1039/c9nr04050a.

[32] Q. Zhou, A. Rahimian, K. Son, D. S. Shin, T. Patel, A. Revzin, Development of an aptasensor for electrochemical detection of exosomes, Methods (2016). https://doi.org/10.1016/j.ymeth.2015.10.012.

[33] W. Zhang, Z. Tian, S. Yang, J. Rich, S. Zhao, M. Klingeborn, P. H. Huang, Z. Li, A. Stout, Q. Murphy, E. Patz, S. Zhang, G. Liu, T. J. Huang, Electrochemical micro-aptasensors for exosome detection based on hybridization chain reaction amplification, Microsystems Nanoeng. (2021). https://doi.org/10.1038/s41378-021-00293-8.

[34] L. Zhuang, Q. You, X. Su, Z. Chang, M. Ge, Q. Mei, L. Yang, W. Dong, L. Li, High-performance detection of exosomes based on synergistic amplification of amino-functionalized Fe_3O_4 nanoparticles and two-dimensional MXene nanosheets, Sensors (2023). https://doi.org/10.3390/s23073508.

[35] J. L. Zhang, M. H. Chang, X. Shi, X. Zhou, Exo-III enzyme based colorimetric small extracellular vesicles (sEVs) detection via G-quadruplex-based signal quenching strategy, Microchem. J. (2022). https://doi.org/10.1016/j.microc.2022.107419.

[36] H. Chen, L. Yuan, W. Song, Z. Wu, D. Li, Biocompatible polymer materials: Role of protein-surface interactions, Prog. Polym. Sci. (2008). https://doi.org/10.1016/j.progpolymsci.2008.07.006.

[37] M. Zarubin, E. Andreev, E. Kravchenko, U. Pinaeva, A. Nechaev, P. Apel, Developing tardigrade-inspired material: Track membranes functionalized with Dsup protein for cell-free DNA isolation. Biotechnol. Prog. (2024). https://doi.org/10.1002/BTPR.3478.

[38] L. P. Kristensen, L. Chen, M. O. Nielsen, D. W. Qanie, I. Kratchmarova, M. Kassem, J. S. Andersen, Temporal profiling and pulsed SILAC labeling identify novel secreted proteins during *ex vivo* osteoblast differentiation of human stromal stem cells, Mol. Cell. Proteom. (2012). https://doi.org/10.1074/mcp.M111.012138.